Desalination and Water Treatment
www.deswater.com

doi: 10.5004/dwt.2021.26554

210 (2021) 54–69
January

CFD modeling of a gravel coarse aggregate sensible heat storage assisted single slope solar still

R. Dhivagar[a,*], M. Mohanraj[a], K. Hidouri[b], M. Midhun[c]

[a]*Department of Mechanical Engineering, Hindusthan College of Engineering and Technology, Coimbatore – 641032, India, emails: dhivagar.papers@gmail.com (R. Dhivagar), mohanrajrac@yahoo.co.in (M. Mohanraj)*
[b]*Engineers National School of Gabes, Analysis Process Unit, Gabes University, Omar Ibn El Khattab Street,6029 Gabes, Tunisia, email: khaoula2013@yahoo.fr (K. Hidouri)*
[c]*Counsil of Scientific and Industrial Research, National Institute for Interdisciplinary Science and Technology, Thiruvanathapuram – 695019, India, email: midhun450450@gmail.com (M. Midhun)*

Received 15 April 2020; Accepted 6 September

ABSTRACT

Solar still desalination is the well-established technology for producing potable drinking water. Many research initiatives have been made on performance improvements in solar stills. This study is intended to improve the efficiency of single slope solar still using a gravel coarse aggregate as sensible heat storage material. In order to achieve this, the inlet saline water was preheated using gravel coarse aggregate before entering into the solar still basin. The results observed from this gravel coarse aggregate assisted solar still (CASS) has been compared with conventional solar still (CSS) experimentally under the same climate conditions of Coimbatore city. Furthermore, the computational fluid dynamics model has been developed for predicting the performance of CASS. The two-phase – three-dimensional model has been developed using ANSYS FLUENT v19.2 software. The analysis considered that the system was quasi-steady state and the results were experimentally validated with the maximum deviation of 14%. The results showed that, the maximum energy efficiency of CASS simulation and experimental were about 28.6% and 25.1%, respectively. Moreover, the simulated and experimental observations were followed a similar pattern. This study shows that computational fluid dynamics (CFD) can be used as the major tool for design, parametric analysis, and difficulties removal in solar still construction.

Keywords: CFD; Efficiency; Heat transfer; Productivity; Solar still

1. Introduction

The access to clean water becomes the basic need for humans. The demand for freshwater increases due to the increase in human population all over the world. This demand for freshwater can be reduced by incorporating portable water generators locally. Barrels of wastewater (sewage water) that are being dispersed due to every day activity from houses can be used as the source for these portable water generators. It is essential to recycle the sewage water or to purify the saline water using energy-efficient and environment-friendly approach. Water purification techniques such as simple disinfection treatment, reverse osmosis (RO), and ion exchange water softener process are

* Corresponding author.

largely used worldwide. But each method has their own disadvantages like operation cost, eliminating bacteria, and fluoride content. Furthermore, maintenance is very difficult for these water purification techniques and is quite complicated to carry out at home. Hence, solar desalination is one of the best options for converting saline water as pure water using solar energy. In addition, the main advantage of this process is that it has no maintenance cost and no skilled labor is required.

In recent years, many researchers have been performed that focuses on enhancing the thermodynamic performance of a solar still incorporating various heat storage materials. Suraparaju and Natarajan et al. [1] investigated on the performance of the solar still using fiber and ridge gourd as sensible heat storage material in the basin and found that, the evaporative heat transfer rate was increased significantly when compared to the conventional solar still. Amirkalaei et al. [2] analyzed the performance parameters of the evaporating chamber and observed that, the best condition for producing freshwater was obtained at the injection pressure of 5 bar, the inlet temperature of 70°C, and the nozzle outlet diameter of 0.9 mm with a discharge coefficient of 0.9. Hardik Jani and Kalpesh Modi [3] conducted experiments on a single basin with dual-slope solar still using circular and square cross-sectional fins. They achieved the daily productivity of about 1.49 and 0.96 kg/m^2, respectively, for circular fins and square fins. Dumka et al. [4] evaluated the efficiency of the single slope solar still using cotton bags filled with sand inside the system. They have achieved an enhanced overall efficiency of about 31.3% and 28.9%, respectively, for 40 and 50 kg of basin saline water. Mohamed et al. [5] performed experiments on solar still using basalt stones as sensible heat storage medium and showed the enhanced effectiveness of about 33.7% when compared to the conventional solar still. Kalpesh Modi and Kuldeep Nayi [6] conducted experiments on square pyramid solar still using forced evaporation, condensation, and granite sensible heat storage material. They improved the efficiency of solar still with forced evaporation and granite thermal storage by 61.5% when compared to the conventional solar still. El-Saida et al. [7] investigated the effectiveness of the tubular solar still using porous packed media with wire mesh and observed the daily distillate of about 4.2 kg/m^2 with enhanced efficiency of about 34% when compared to the traditional solar still. In a related work, the effectiveness of the single-slope solar still using a gravel coarse aggregate sensible heat storage material was investigated and reported that there was an enhancement in the overall efficiency of about 11% when compared to the conventional solar still [8]. Zanganeh et al. [9] evaluated the influence of wettability on single slope solar still using a nano-coating at condensing area and enhanced the effectiveness by 23%. Kabeel et al. [10] evaluated the solar still performance with the effect of the graphite nanoparticles and observed the improved efficiency by 65.1% for 20% mass concentrations Gnanaraj and Velmurugan [11] conducted experiments on a double slope single basin solar still using fins, black granite, wick, reflector, internal, and external modifications and improved the efficiency by 58.4%, 69.8%, 42.3%, 93.3%, and 171.4%, respectively, when compared to the conventional solar still. Sakthivel et al. [12] investigated the performance of a solar still in which jute cloth regenerative medium is used to regenerate the latent heat released during condensation of water vapor. It has been reported that, the efficiency and productivity of the solar still were improved by about 8% and 20%, respectively, than the conventional solar still. Similarly, Sakthivel and Arjunan [13] investigated the performance of single slope solar still using cotton cloth as a heat regenerative medium. It was reported that, the maximum energy and exergy efficiency of 23.8% and 2.6%, respectively, was observed for cotton cloth thickness of 6 mm. Kumar et al. [14] reported that, the phase change heat storage has significance on the productivity of single slope solar still during afternoon hours. Comprehensive review of the solar still system [15–17] reported that the productivity of active solar still has enhanced by 120% and 700%, respectively, than conventional solar still.

Many research works also have been concentrating on the solar still augmented with water heater, air heater, PV panel, parabolic trough collectors, heat exchangers, and heat pump. Kabeel et al. [18] conducted performance analysis in a single slope solar still integrating with double pass solar air heater. The double-pass solar air heater preheats the air before entering into the solar still and enhances the water evaporation rate. The productivity of the solar still was improved by 9.4 kg/m^2, which was twice that of the conventional solar still. Belyayev et al. [19] improved the productivity of a heat pump assisted solar still by 80% than the conventional stills. Daily productivity of the system was improved to 12.5 kg/m^2 during summer climate conditions with an efficiency of 62%. In a similar work, the daily distillate of a heat pump compression solar still was enhanced by 12 L/m^2 during sunny days. The improved efficiency of this proposed model was found to be around 20%–80% when compared to the conventional solar still [20]. In recent work, the performance of various configurations of a heat pump assisted solar still was investigated experimentally. It was reported that the heat pump assisted solar still with variable glass position achieved 84.5% of enhanced efficiency when compared to the conventional solar still and also the glass positions played a significant role in productivity [21]. Hassan et al. [22] tested the performance of parabolic trough collector assisted single slope solar still with the sand heat storage medium. They confirmed that, the maximum energy and exergy efficiency of the proposed model was about 216.6% and 325% higher than the simple conventional solar still. The proposed system also has the exergy based CO_2 mitigation of about 5.9 tons/y. Rahbar et al. [23] investigated the performance of the double slope solar still assisted thermoelectric heating modules and observed the maximum exergy efficiency of about 25% during 15:00 h. Rashidi et al. [24] improved the performance of single slope solar still using a reticular porous layer by 17.35% under the climate conditions of Iran. Sasikumar et al. [25] analyzed the passive inclined solar panel basin (PISPB) still at a diversified flow rate of water and found that, at higher flow condition, the still energy and exergy efficiency decreases and it is estimated as 36.06%, 25.56% and 16.95% and 2.97%, 1.91%, and 1.01%, respectively, for flow rates of 4.68, 7.56, and 10.08 kg/h. Manokar et al. [26] conducted experiments on active inclined solar panel basin solar still and observed that the maximum freshwater yield at 1.8, 3.2, and 4.7 kg/h was

7.5, 6.5, and 5.4 kg, respectively. The daily average thermal and exergy efficiency of the proposed model at 1.8, 3.2, and 4.7 kg/h is 43.71%, 38.27%, and 29.62% and 8.39%, 6.94%, and 5.08%, respectively.

The performance of solar stills have been evaluated in terms of numerical aspects to quantify the energy conversion and energy losses in the solar still. Rashidi et al. [27] investigated the partitioning solar still performance numerically and experimentally in Iran climatic conditions. The numerical simulation based simple algorithm was utilized to enhance the productivity by 4.81%, 4.82%, 5.62%, and 8.16% for 1st, 2nd, 3rd, and 4th days of the experiment, respectively. In related work, an optimization procedure was performed by response surface methodology (RSM) to optimize the position and size of the partition inside the solar still. The results revealed that, the real optimized parameters for the maximum normalized Nusselt number of bottom installed partition are $X' = 0.23$ and $Y' = 0.18$ [28]. El-Sebaii et al. [29] investigated the transient mathematical models of solar still using phase change materials and reported that the evaporative heat transfer coefficient was improved by 27%. Rashidi et al. [30] examined the performance of the modified solar still using the volume-of-fluid model and found that the volume-of-fluid model was better than the moist air model. The results revealed that, the modified solar still has enhanced productivity of about 39% when the sponge rubber porous layer was used in the solar still basin. Rashidi et al. [31] performed the numerical study to investigate the effect of nanofluid on the performance of stepped solar still. The results showed that, there was only 2.1% difference between the estimated results by RSM and calculated results by computational fluid dynamics (CFD). Radhwan [32] studied the experiments on stepped solar still built-in latent heat thermal energy storage by analyzing the transient performance and reported efficiency of the system has increased about 57%. Chamkha et al. [33] examined the airflow in a semi-infinite vertical plate in the presence of radiation effect and concluded that, the velocity and temperature decreased as the distance from the plate's leading edge was increased. They also found that, the increase in the radiation parameter led to decreases in both the velocity and temperature but an increase in the concentration [34]. Chamkha [35] performed the numerical study on the effect of charging and discharging period of the phase change materials and found that, the amount of saved energy within the PCM was about 41.6%. Ahmed et al. [36] performed simulations on multistage evacuated solar still using two dimensional CFD model and showed that the maximum evaporative heat transfer occurs under vacuum conditions. Rahbar et al. [37] estimated the enhanced convective heat transfer coefficient in a tubular solar still by CFD model and reported that, the productivity of solar still was improved by 250% when water temperature increased. Rashidi et al. [38] simulated the performance of solar still using nano fluids by VOF model and showed that, the viscous and thermal entropy has increased the productivity by about 95% and 25%, respectively. Panchal and Patel [39] investigated the various parameters of solar still using CFD model and revealed that, the evaporative heat transfer was a major factor that influenced the thermal performance of the system. Khare et al. [40] improved the performance of a solar still using various quantities of water and reported that, 5 L water quantity has enhanced efficiency by about 32% and there was a good agreement between experimental and CFD results. Taamneh [41] improved the performance of solar still using Jordanian zeolite and proved that, there was an acceptable solution between experimental and CFD results.

The above literature review showed that, numerous investigations have been reported on performance enhancement of solar still with different configurations. However, there is no specific research work has been reported on CFD analysis of CASS. The main objective of this work is to analyze the effect of heat transfers on productivity when preheated feed water used in CASS. Hence, an attempt has been made in this research work to develop a three dimensional two phase model solar still using CFD technique. The model of the solar still has been generated and simulated on ANSYS FLUENT v19.2 software. Simulated results of performance parameters are compared with experimental data of CASS. They were in a good agreement and applicable to design the optimal system.

2. Experiment analysis

The experimental studies have been performed under the same climatic conditions of Coimbatore city (latitude: 11°01′68″N and longitude: 76°95′58″E), in India.

2.1. Experimental setup

Figs. 1a and b depict the schematic and photographic view of CASS, respectively. The experimental setup consists of coarse aggregate sensible heat storage, water storage tank of 20 L capacity, and solar still of basin area 0.78×0.65 m^2. The walls and basin of a solar still are manufactured from 1.2 mm thickness of iron sheet. The basin of a solar still was coated with black paint to enhance the absorption coefficient. The top section of the solar still was covered with 3 mm thick glass plate with a maximum transmission coefficient of more than 0.95 and minimum absorption coefficient of less than 0.1. The silicon rubber seals have been used to fix the glass plate and to reduce the water vapor leakage from the solar still. The sides of solar still were insulated with 25 mm thick thermocol to reduce the heat loss. A collection tray was placed over the bottom surface of the glass to collect the condensate. About 42 kg of coarse aggregate sensible heat storage materials with 15 cm bed thickness was used in this work. The thermal properties of sensible heat storage materials reported in the open literature are given in Table 1. It is confirmed that, coarse aggregate is having high thermal storage capacity when compared to other sensible heat storage medium. During sunshine hours, the solar energy was harvested directly to the basin of a solar still and also by the coarse aggregate sensible heat storage medium. The coarse aggregate medium preheats the saline water before entering into the solar still. The flow control valves have been used to control the water flow rate passing through the coarse aggregate. The water level in the basin was monitored at every hour interval and maintained the consistent range. The salt deposition in the basin was removed periodically.

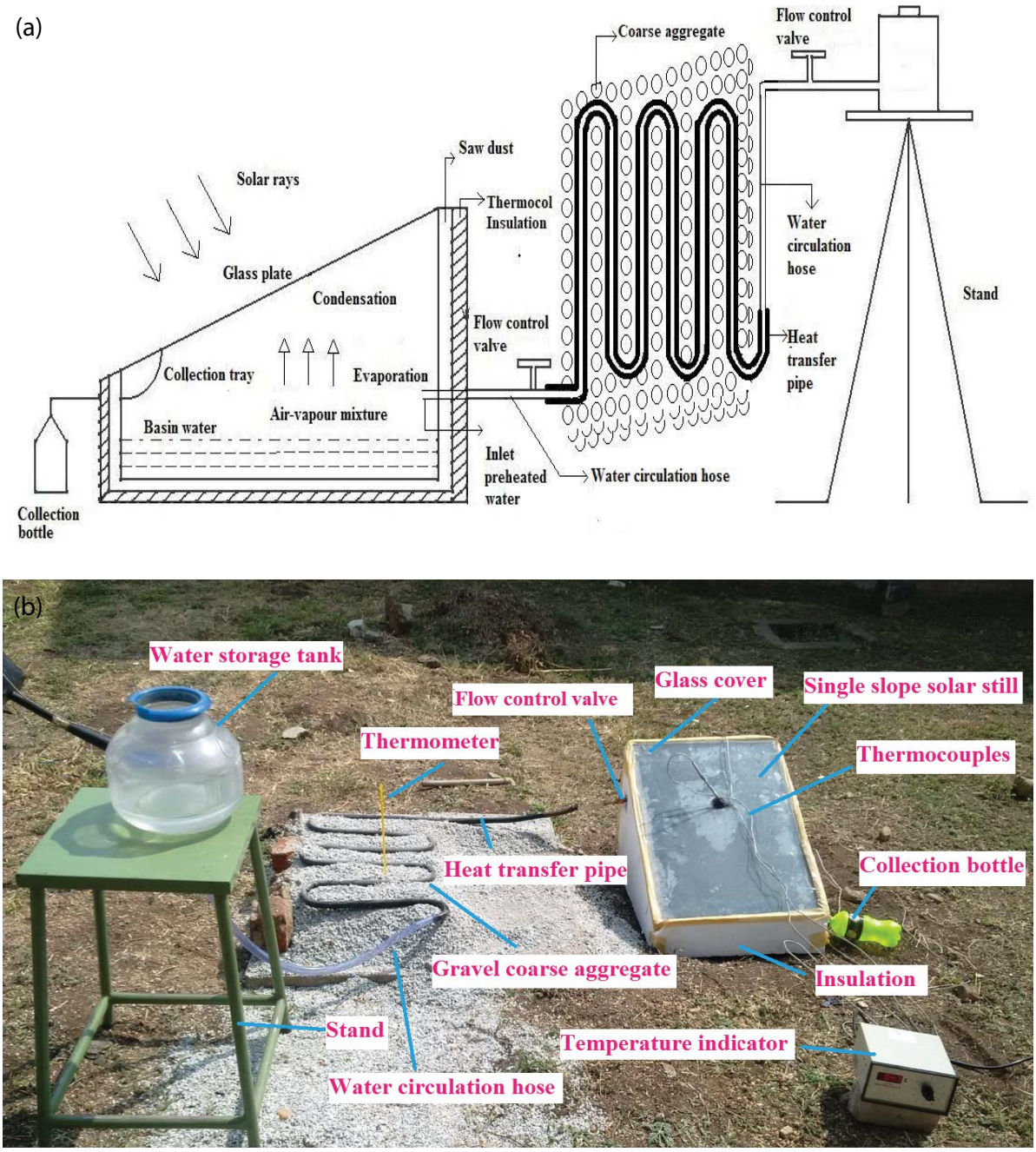

Fig. 1. (a) Schematic view of solar still and (b) photograph of experimental setup.

2.2. Instrumentation

The detailed specifications of measuring devices used in experimental are listed in Table 2. Eight calibrated *K*-type thermocouples have been used to measure the temperature of water in the basin, the temperature of air-water vapor mixture, the glass temperature bottom surface of the solar still, and sidewalls of the solar still, inlet and outlet of gravel coarse aggregate and gravel bed. All the thermocouples were connected to a digital temperature indicator of ±0.2°C. The ambient temperature was measured using a calibrated thermometer with an accuracy of ±0.2°C. The ambient wind velocity was measured using a cup type anemometer with ±0.1 m/s. The solar irradiation falls on the solar still was measured using solar intensity meter with ±5 W/m^2. The output of the solar still was measured using a calibrated beaker. The water level in the solar still was measured using a measuring scale with the least count of 1 mm.

2.3. Experimental procedure

The experimental observations have been made in CASS under the weather conditions of Coimbatore city. Before experimental observations, the basin was filled with

Table 1
Thermal properties of different sensible heat storage materials

S. No	Materials	Thermal conductivity (W/m K)	Thermal diffusivity (mm^2/s)	Specific heat capacity (kJ/kg K)	Water absorption rate (%)
1	River sand	1.62	0.35	0.83	9.6
2	Charcoal	0.12	0.1	0.81	12
3	Clay soil	1.49	0.16	0.79	5.8
4	Coarse aggregate	2.25	0.42	0.86	0.5

Table 2
Uncertainties of measuring instruments

S. No	Instrument	Range	Observed error %	Standard uncertainty
1	Thermometer	0°C–100°C	1.2	±0.57°C
2	*K*-type thermocouple	0°C–600°C	1.5	±0.65°C
3	Solar intensity meter	0–2,500 W/m^2	3.1	±0.5 W/m^2
4	Measuring jar	0–1,000 mL	5.2	±3.77 mL

the required quantity of water and allowed the solar still to warm up and attain steady-state with ambient conditions. The glass surface was cleaned using a soft cloth to remove the dust accumulation, which may influence the performance of the solar stills. During experimental observations, the solar irradiance, ambient temperature, and temperatures at all the typical locations in the solar still were measured at every 1 h interval from 9.00 to 18.00 h. The water level in the basin of a solar still was monitored every 1 h interval and maintained low water depth using flow control valves. The productivity of the solar still at every 1 h was monitored using a calibrated jar. Ten experimental trials have been made to check the consistency of the experimental results. The experimental observations have been tabulated and the energy performance was evaluated. Finally, the results were compared with CSS.

2.4. Uncertainty analysis

In this work, the uncertainties occurring in measuring instruments during the experiment are studied. The uncertainties of directly measured variables such as productivity and temperature, consider the sources of errors, random and systematic. The errors in calculating parameters are estimated using the following relation [42]:

$$w_r = \left[\left(\frac{\partial R}{\partial x_1}w_1\right)^2 + \left(\frac{\partial R}{\partial x_2}w_2\right)^2 + \ldots\ldots\ldots + \left(\frac{\partial R}{\partial x_n}w_n\right)^2\right]^{1/2} \quad (1)$$

Here is a given function, w_r are the total uncertainty, X_1, X_2, ... X_n are the independent variables, w_1, w_2, ...w_n are the uncertainty in the independent variables.

An uncertainty of measuring instruments is given in Table 2. From the Eq. (1), the uncertainty of energy efficiency is found to be 2.1%.

3. Mathematical model

The important parameters that influenced the performance of the solar still were identified to be internal heat and mass transfer coefficients. Such parameters depend on the modes of heat transfer occurring in the solar still. The distillate rate is directly proportional to the effectiveness of the three heat transfers. For analyzing water and air vapor mixture in the solar still, a two-phase model was created in the volume of fluid framework using quasi steady-state condition. Hence, the surface evaporation of liquid was only considered for the modeling. The turbulence models were considered as the saline water assumed to be stagnant inside the solar still. In this work, energy and mass transfer have been considered for simulation purpose. Hence, the time and volume-average continuity, energy, and mass equations are numerically solved for each phase.

3.1. Governing equations

The following assumptions were taken into account when evaluating the energy balance equation [40].

- No vapor leakage in the solar still.
- The heat capacity of cover, absorbing material, and insulation is negligible.
- The temperature gradient across the glass cover and the basin saline water is zero.
- The depth of basin saline water is constant.
- The radiation, convective, and evaporative heat losses are linear with the temperature.

The following model equations are based on the continuity, momentum, energy, and mass transfer conservation principles at steady-state conditions.

The energy equation for the gas phase is given by [43]:

$$\nabla\cdot\left(r_G\,\rho_G V_G H_G\right) = -\nabla\cdot q + \left(Q_{LG} + S_{LG}H_{LG}\right) \quad (2)$$

The energy equation for the liquid phase is given by [43]:

$$\nabla\cdot\left(r_L\rho_L V_L H_L\right)=-\nabla\cdot q-\left(Q_{\mathrm{LG}}+S_{\mathrm{LG}}H_{\mathrm{LG}}\right) \tag{3}$$

The above equations are associated with energy and mass transfer between two phases and must satisfy the local balance conditions.

$$Q_{\mathrm{LG}}=-Q_{\mathrm{GL}} \tag{4}$$

The continuity equation for gas phase is given by [43]:

$$\nabla\cdot\left(r_G\rho_G V_G\right)+S_{\mathrm{LG}}=0 \tag{5}$$

The continuity equation for liquid phase is given by [43]:

$$\nabla\cdot\left(r_L\rho_L V_L\right)-S_{\mathrm{LG}}=0 \tag{6}$$

The local balance condition must be satisfied by phases occurs during mass transfer.

$$S_{\mathrm{LG}}=-S_{\mathrm{GL}} \tag{7}$$

The momentum equation for gas phase is given by [43]:

$$\nabla\cdot\left(r_G\left(\rho_G V_G V_G\right)\right)=-r_G\nabla P_G+\nabla\cdot\left(r_G\mu_{\mathrm{laminar},G}\left(\nabla V_G+\nabla V_G^T\right)\right)+ r_G\rho_G g_r-M_{\mathrm{GL}} \tag{8}$$

The momentum equation for the liquid phase is given by [43]:

$$\nabla\cdot\left(r_L\left(\rho_L V_L V_L\right)\right)=-r_L\nabla P_L+\nabla\cdot\left(r_L\mu_{\mathrm{laminar},L}\left(\nabla V_L+\nabla V_L^T\right)\right)+ r_L\rho_L g_r+M_{\mathrm{GL}} \tag{9}$$

The drag coefficient of the interfacial force was assumed to be 0.44. The mass transfer equation for the gas phase is given by [43]:

$$\nabla\cdot\left[r_G\left(\rho_G V_G Y-\rho_G D_G\left(\nabla Y\right)\right)\right]-S_{\mathrm{LG}}=0 \tag{10}$$

The mass transfer equation for liquid phase is given by [43]:

$$\nabla\cdot\left[r_L\left(\rho_L V_L X-\rho_L D_L\left(\nabla X\right)\right)\right]+S_{\mathrm{LG}}=0 \tag{11}$$

The volume conservation equation for both phases is given by [43]:

$$r_G+r_L=1 \tag{12}$$

3.2. Heat transfer mechanism

For modeling the heat transfer processes, the following equations are used. The overall heat transfer coefficient for water and glass is given by [44]:

$$U_{o\,w-g}=\left(h_{c\,w-g}+h_{\mathrm{eva}\,w-g}+h_{r\,w-g}\right) \tag{13}$$

The convective heat transfer coefficient is given by [44]:

$$h_{c\,w-g}=0.884\left[T_w-T_g+\frac{\left(P_w-P_g\right)T_w+273}{268{,}900-P_w}\right]^{1/3} \tag{14}$$

Here, P_g and P_w are:

$$P_g=\exp\left[25.317-\frac{5{,}144}{T_g+273}\right] \tag{15}$$

$$P_w=\exp\left[25.317-\frac{5{,}144}{T_w+273}\right] \tag{16}$$

The evaporative heat transfer coefficient is given by [44]:

$$h_{\mathrm{eva}\,w-g}=0.016h_{c\,w-g}\frac{\left(P_w-P_g\right)}{\left(T_w-T_g\right)} \tag{17}$$

The radiative heat transfer coefficient for water to glass is calculated using the following relation [45]:

$$h_{r\,w-g}=\sigma\varepsilon_{\mathrm{eff}}\left[\left(T_w+273\right)^2-\left(T_g+273\right)^2\right]\left(T_w+T_g+546\right) \tag{18}$$

Here,

$$\varepsilon_{\mathrm{eff}}=\frac{1}{\left[\frac{1}{\varepsilon_w}+\frac{1}{\varepsilon_g}-1\right]} \tag{19}$$

The latent heat of water during its evaporation is given by [46]:

$$L=2.4935\times10^6\times\left[\begin{matrix}1-9.4779\times10^{-4}\times T_w+1.3132\times10^{-7}\times\\ T_w^2-4.794\times10^{-9}\times T_{\boldsymbol{w}}^3\end{matrix}\right] \tag{20}$$

The hourly yield of the solar still is given by [46]:

$$m_w=\frac{h_{\mathrm{eva}\,w-g}\left(T_w-T_g\right)\times3{,}600}{L} \tag{21}$$

The energy efficiency of the system is given by [42]:

$$\eta_E=\frac{m_w\times L}{A_{\mathrm{ss}}\times\sum I_{\mathrm{ss}}\times3{,}600} \tag{22}$$

4. Flow geometry

The dimensional details of single slope solar still and heat transfer pipe is shown in Figs. 2a and b. The solar still glass cover was titled at an angle of 45°. The system was located along the east-west direction by facing toward the south direction to maximize the absorption of solar irradiation and basin saline water was maintained at 1 cm depth. A three-dimensional unstructured meshes and model

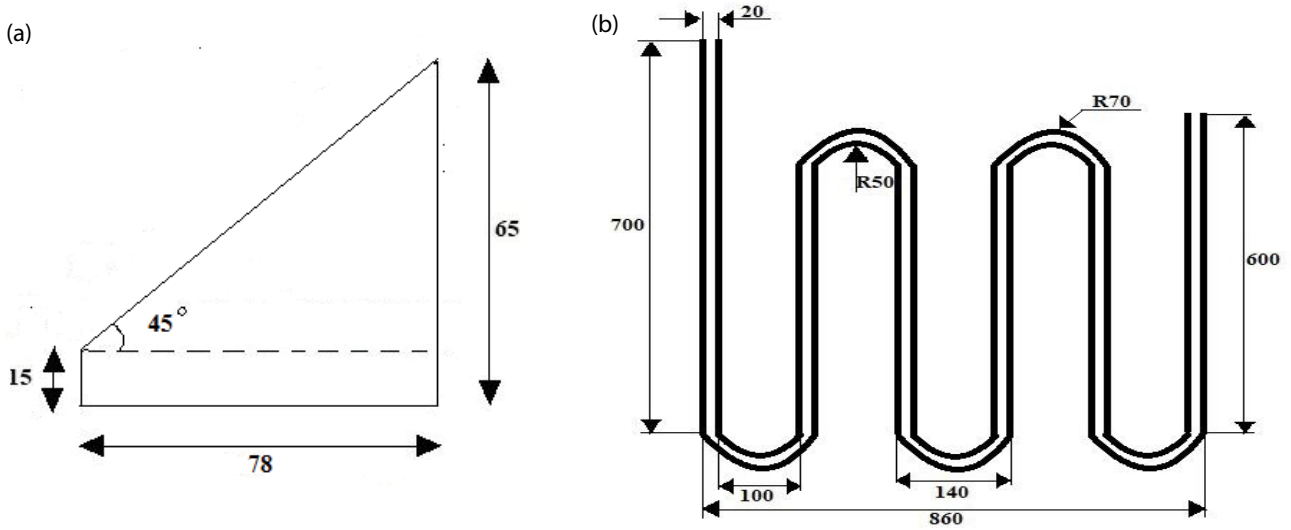

Fig. 2. Dimensions of (a) solar still in cm and (b) heat transfer pipe in mm.

geometry of the solar still and the heat transfer pipe is shown in Figs. 3a–d, respectively. The grid independence test was performed to identify the quality of mesh size in this model. The convergence criteria were achieved for all the equations at each time step. Until the criterion was satisfied, the grid size was identified through increasing the number of meshes.

4.1. Boundary and initial conditions

The quantity of solar irradiation in the solar still largely depends on the absorptivity and transmissivity of the glass cover. The initial water level is considered to be 1 cm for simulation purpose. The water and vapor volume fractions were assumed as 0.06 and 0.94, respectively. According to the experimental data, the initial water temperature and the amount of solar irradiation received by the solar still is calculated in every 1 h. As the volume of water increases, the evaporation decelerates. Hence, the water level is balanced with respect to pressure for the remaining levels. In other words, the pressure of the system was defined as being directly proportional to the water level of a solar still, based on hydrostatic pressure.

Appropriate boundary conditions for solving the continuity and momentum equations were defined at all boundaries. Despite of a high number of time steps and computer time constraints, CFD simulation had run time of 14 h. It was assumed that for 1 h, the received solar irradiation by the basin as well as water and glass temperatures were based according to the solar calculator in fair weather condition. Constant temperature boundary conditions were enforced on glass cover, basin, and collection tray [40]. The experiment was performed from 9:00 to 18:00 h. During each 1 h time interval, an average temperature was set as the boundary condition. Solar irradiation was based upon the absorption factor and emissivity of the glass cover, saline water, and basin. Hence, basin of the solar still and the coarse aggregate temperature were kept as equal. For drop formation on the glass cover, adhesion forces were taken into account in the simulations [43]. The side walls were assumed as adiabatic wall, hence no heat losses occur in the solar still to ambient. It assumes that, distillate collected in collection bottle is equal to evaporation takes place inside the solar still. For effective simulation, adiabatic condition is required, which prevents the heat transfer losses. For the liquid phase, no-slip wall boundary condition was specified and free-slip boundary condition was used in the gas phase [43].

4.2. Solution initialization

To convert the governing equations into numerically solvable algebraic equations, ANSYS FLUENT v19.2 has been used in the study, which works on the finite volume method. The following assumptions are made to study the numerical work [40]:

- During the heat transfer process, the thermo-physical properties of the iron sheet, copper, glass, and air are remaining constant.
- There are perfect thermal contact between glass cover, solar still basin walls, and its surrounding.
- The wall temperature of a solar still is considered equal and undisturbed.

5. Results and discussion

The results observed in CFD simulation and experimental are discussed in the section.

5.1. Simulation results

ANSYS FLUENT solver v19.2 has been used to carry out CFD analysis for solving the equations. The computation time per simulation needed around 4–14 h to attain the quasi steady-state condition. This depends on the system that is being used for computational analysis. Tetrahedral

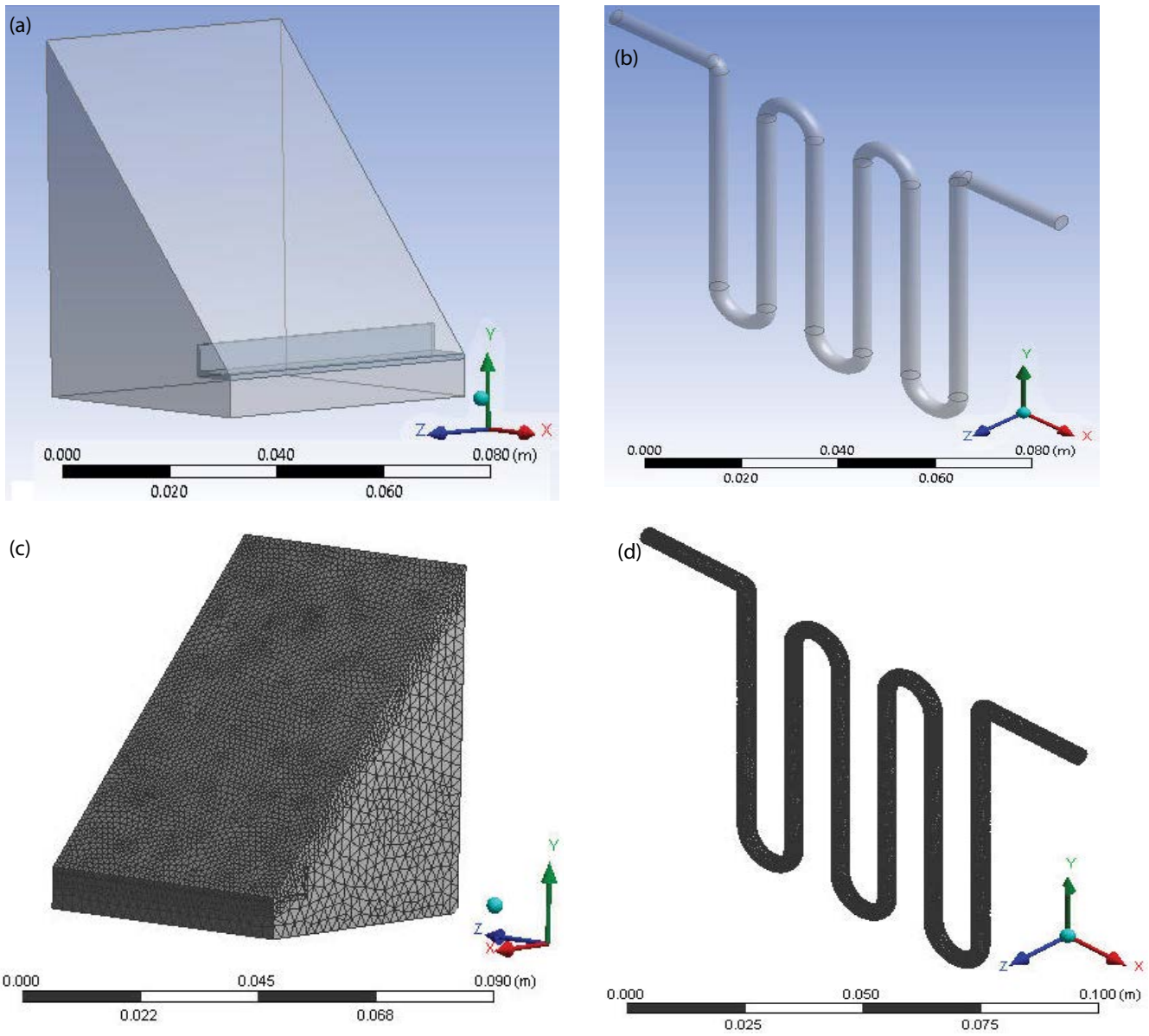

Fig. 3. Model geometry of (a) solar still, (b) heat transfer pipe. Unstructured model mesh of (c) solar still, and (d) heat transfer pipe.

type of unstructured mesh has been used in this work. Air was considered as an ideal fluid in this simulation because of its thermal conductivity and viscosity vibrational character with temperature. Hence, the Rayleigh number for the simulation was set 1,200 [47]. The sensitivity of the simulation result is very important for optimum analysis, and it can be checked by grid size, hence by checking the results of 21,181; 34,312; 49,207; 75,413; and 92,137 cells, with increasing numbers of grids, the simulation results became closer to experimental results.

Fig. 4a depicts the condensed water droplets on the glass cover. It is observed that, the volume fraction of droplet on glass cover was very low when compared with its surface. Hence, the legend range of the contour between 0 and 1×10^{-4} was recommended for a proper representation of condensed droplets [43,48]. The red and yellow colors are shown that, the more condensed water droplets were formed on the glass cover. This happens due to the usage of the preheated saline water in the solar still basin. Water volume fraction contours on collection tray and side view of the solar still are shown in Figs. 4b and c, respectively. From Fig. 4b, it is observed that, the maximum water droplets were collected in the tray. The red color indicates that, the more quantity of condensed droplets fell down in the tray due to sliding contact of the glass cover and gravitational force. This enhancement also occurs with the usage of preheating technique. From Fig. 4c, it is seen that, the interface of phases was distinct and completely apart. Hence, only the liquid phase occurs in the glass cover, collection tray and the basin of the model geometry. The influence of gas mixture temperature of the solar still is depicted in Fig. 4d. It is observed that, the gas mixture temperature was mostly

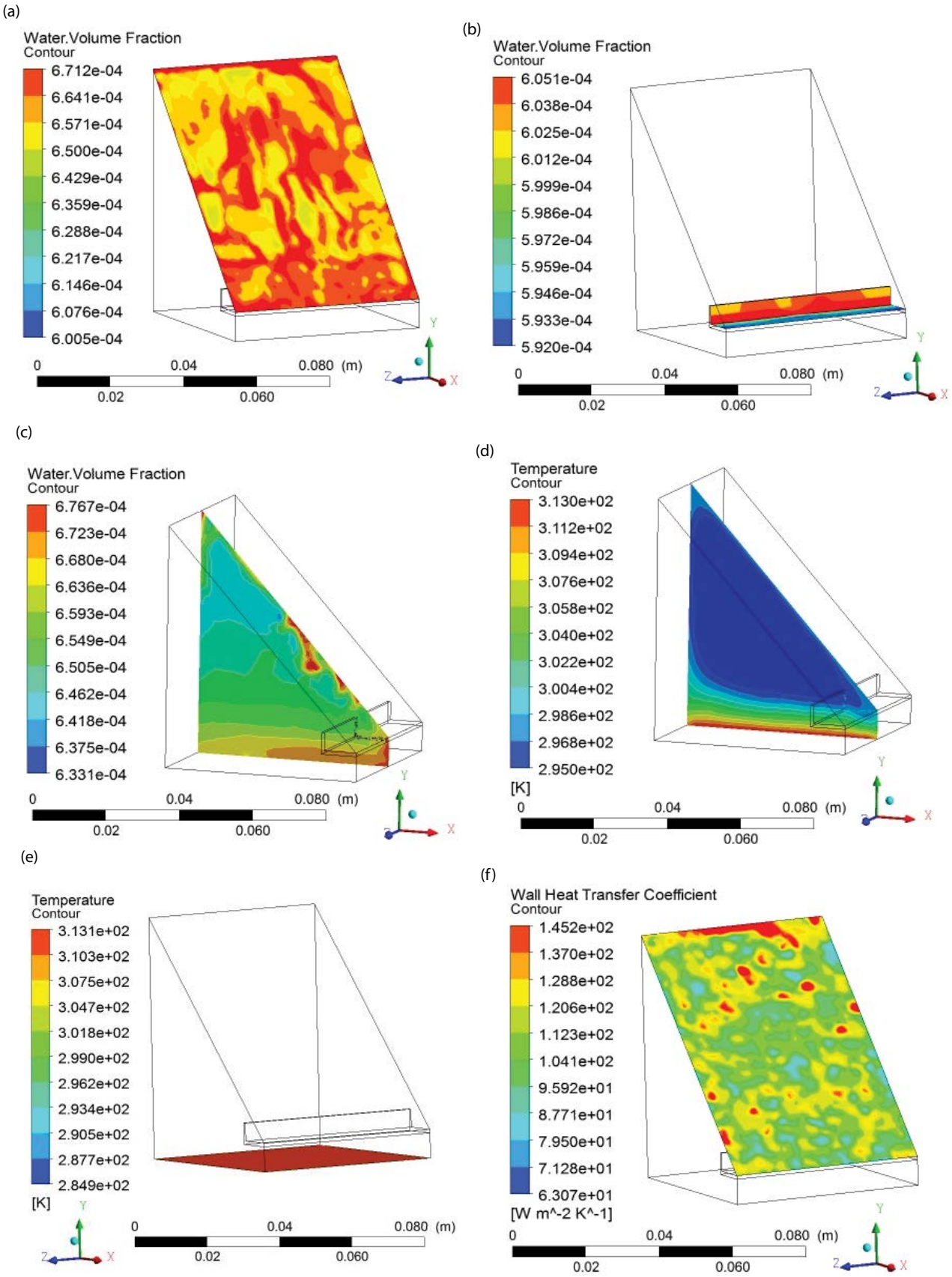

Fig. 4. Water volume fraction contour on (a) glass cover, (b) collection tray, (c) water volume fraction contour at side view, (d) gas mixture temperature contour, (e) basin temperature of solar still, and (f) glass heat transfer coefficient on solar still.

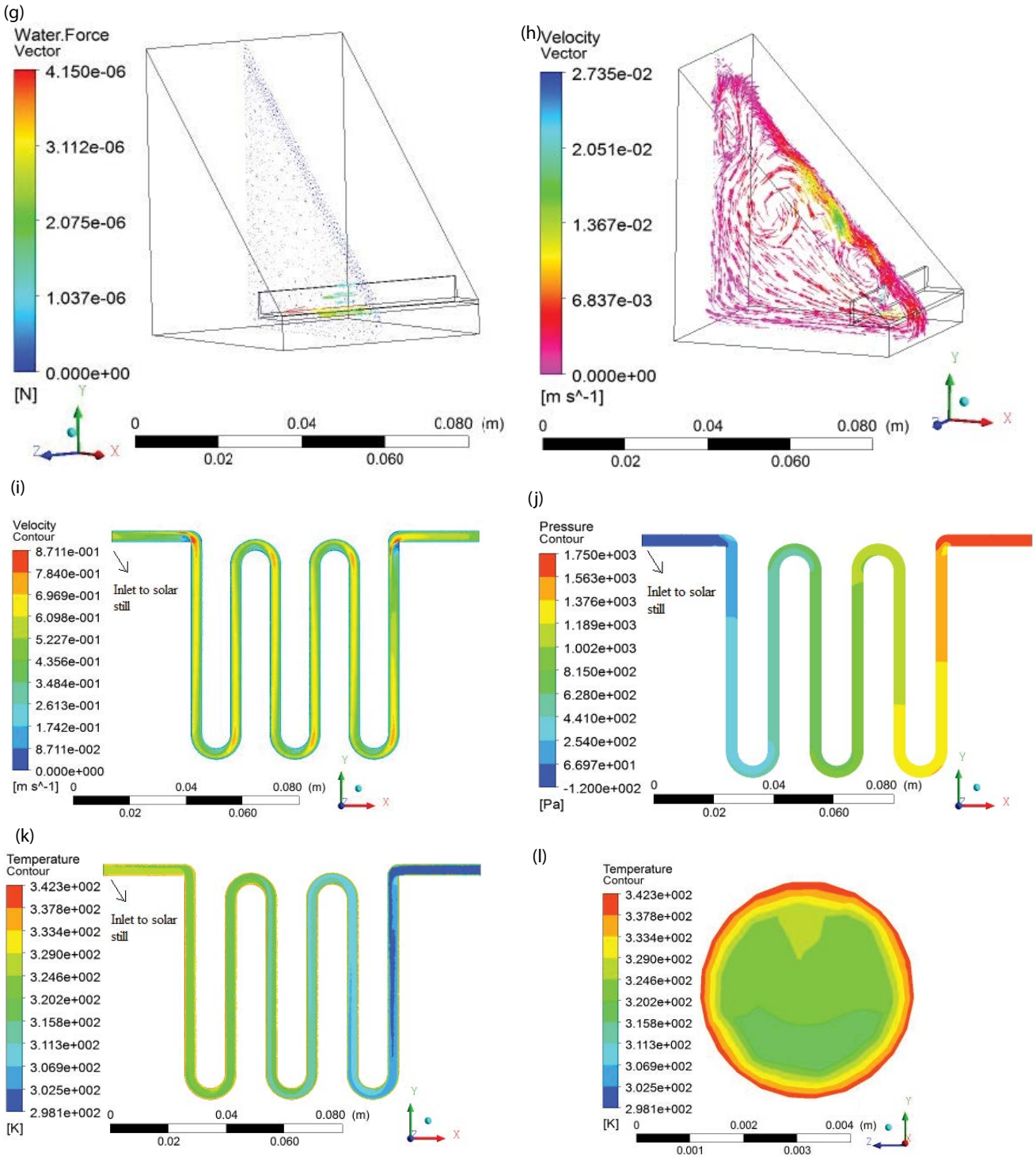

Fig. 4. (g) Water force vector on solar still, (h) gas mixture velocity on solar still, (i) saline water velocity on heat transfer pipe, (j) saline water pressure on heat transfer pipe, (k) saline water temperature on heat transfer pipe, and (l) cross-sectional view of saline water temperature at pipe inlet to the solar still.

same in every region in the solar still. It was not varied that much effectively from the bottom of the glass cover to certain distance toward to the basin area. But there was a slight variation in and around the regions of the basin as color changes. The basin temperature of the still is illustrated in Fig. 4e. It is observed that, the basin temperature was enhanced due to the preheated water used in the solar still. It was improved from the basin area to a certain distance of the solar still walls. Then it was reduced towards to the glass cover as solar irradiation reduces. The glass wall heat

transfer coefficient on solar still is indicated in Fig. 4f. It is observed that, the rate of solar irradiation striking on the glass cover was not much effective due the refraction of glass cover to the atmosphere. Sometimes, solar irradiations are fully reflected in the atmosphere without absorbed by the glass cover. Wind velocity and relative humidity (moisture content in the atmospheric air) are playing the important role to minimize the glass absorptivity in sunshine hours [42]. Fig. 4g illustrates the water force vector on the solar still. It is observed that, the water (air-vapor) force was not much impact at the bottom of the glass cover due to the higher temperature release. But, it was higher in the basin of the solar still, particularly on the surface layer of the saline water. The red and yellow colors indicating that there was higher in the water force (air-vapor). It happens due to the buoyancy effect and convective heat transfer at the water surface [16]. Fig. 4h shows the gas mixture velocity on solar still. It is observed that the gas phase travels on circular motion between the glass cover and basin. It is also seen that, the warm phase goes upward with the buoyancy force and condenses on the glass cover, then comes down and forces the lighter warm phase toward the glass cover due to free convective heat transfer [43].

Preheated saline water velocity in the heat transfer pipe is depicted in Fig. 4i. It is observed that, the saline water velocity increases in the bending portion due to pressure gradient reduce. Apart from this, the velocity of the saline water was not varying that much effectively at any locations of the heat transfer pipe. The pressure and temperature of the saline water increase in the mode of conduction and convection due to the heat accumulated in the coarse aggregate [16]. The increase in pressure was influencing the saline water velocity in the heat transfer pipe except for the bending portion. However, the velocity of saline water is minimized at the solar still inlet due to maintain the lower water depth. Fig. 4j illustrates the pressure regions on the heat transfer pipe. It is observed that, the maximum saline water pressure occurs in the pipe where the water supply starts. It increases gradually due to the heat transfer from the coarse aggregate and reduces slowly when heat losses to the surroundings [42]. It also reduces as velocity increase at the bending portion. It is understood that, the velocity was influencing the saline water pressure only at the bending portion of the heat transfer pipe. Preheated saline water temperature in the pipe is depicted in Fig. 4k. It is observed that, the temperature of saline water was minimum where the water supply starts. It increases gradually to the inlet portion of solar still due to the thermal energy stored in coarse aggregate. The temperature and pressure are nearly following the same patterns in the heat transfer pipe. But the saline water temperature was improved significantly at the wall side entirely when compare to mid-portion of the heat transfer pipe. It happens due to the force of the convective heat transfer (convective heat transfer coefficient) reduces as a water thickness increase in the pipe [42]. The cross-sectional view of saline water temperature at pipe inlet to the solar still is also depicted in Fig. 4l. It is understood that, the maximum temperature occurs in the sidewall of the pipe due to the conductive and convective heat transfers. The accepted fact is that, the heat was not transferred to the full area of the pipe and heated the water completely. It may happen due to the heat losses from the pipe and coarse aggregate to the surroundings [8]. The influence of friction in the pipe also was the reason for the temperature, pressure, and velocity losses [42].

5.2. Validations of CFD results

This research work aims at CFD modeling of evaporation and condensation processes which occur in solar stills. Saline water inside the solar still vaporizes by solar energy. The difference in temperature among water vapor and glass cover leads to vapor condensation on the glass surface. The droplets fall down and collect in the collection tray. For the freshwater calculation in simulations, the quantity of accumulated water on the collection tray was considered as the rate of water production. In this section, the simulation results are compared with experimental observation taken from CASS. Furthermore, CSS results are plotted to estimate the experimental performance of CASS.

The variation of solar irradiation and ambient temperature is illustrated in Fig. 5a. In CFD simulation, as expected, the solar irradiation was increasing during the morning hours and reaches the maximum value of about 895.3 W/m^2 during noon hours. In experiments, the maximum solar irradiation was observed about 842.2 W/m^2 for both CASS and CSS. During evening hours, the solar irradiation was decreased in both simulation and experimental. Despite of the sunshine period was found to be around 12 h during the daytime, the successful sunshine availability (above 250 W/m^2) for the experiment was only about 8–10 h. Even though the solar irradiation observation does not exactly same in both simulation and experimental, they do follow the similar patterns. This happens due to the intensity of solar irradiations taken in the simulation doesn't account for natural attenuation [43,49]. The deviation between simulation and experimental solar irradiation was observed to be about 8.01%. For the variation of ambient temperature, in simulation results, it is observed that, the ambient temperature increases in noon hours and reaches the maximum value of about 40.2°C whereas the maximum temperature in experimental was observed about 38.9°C in both CASS and CSS. During evening hours, it falls down as solar irradiations reduce. However, the flow patterns do follow the same path and the deviation between simulation and experimental results were found to be about 3.6%.

Fig. 5b shows the effect of glass and basin temperature for simulation and experimental. It is observed that, the glass temperature of both simulation and experimental results do follow similar patterns. The maximum glass temperature of simulation and experimental were about 62.1°C and 59.4°C (both CASS and CSS), respectively. During evening hours, it falls down as solar irradiation and ambient temperature reduce. It is also observed that, there was 4.4% deviation between simulation and experimental results. For basin temperature, it is observed that, the maximum temperature of 51.4°C found during 13:00 h in simulation. The experimental basin temperature of both CASS and CSS are observed to be about 49.1°C and 46.9°C, respectively during 13:00 h. It is seen that, the CASS basin temperature is 4.3% higher than the CSS. The reason behind the enhancement of CASS was the effect of the preheated saline water

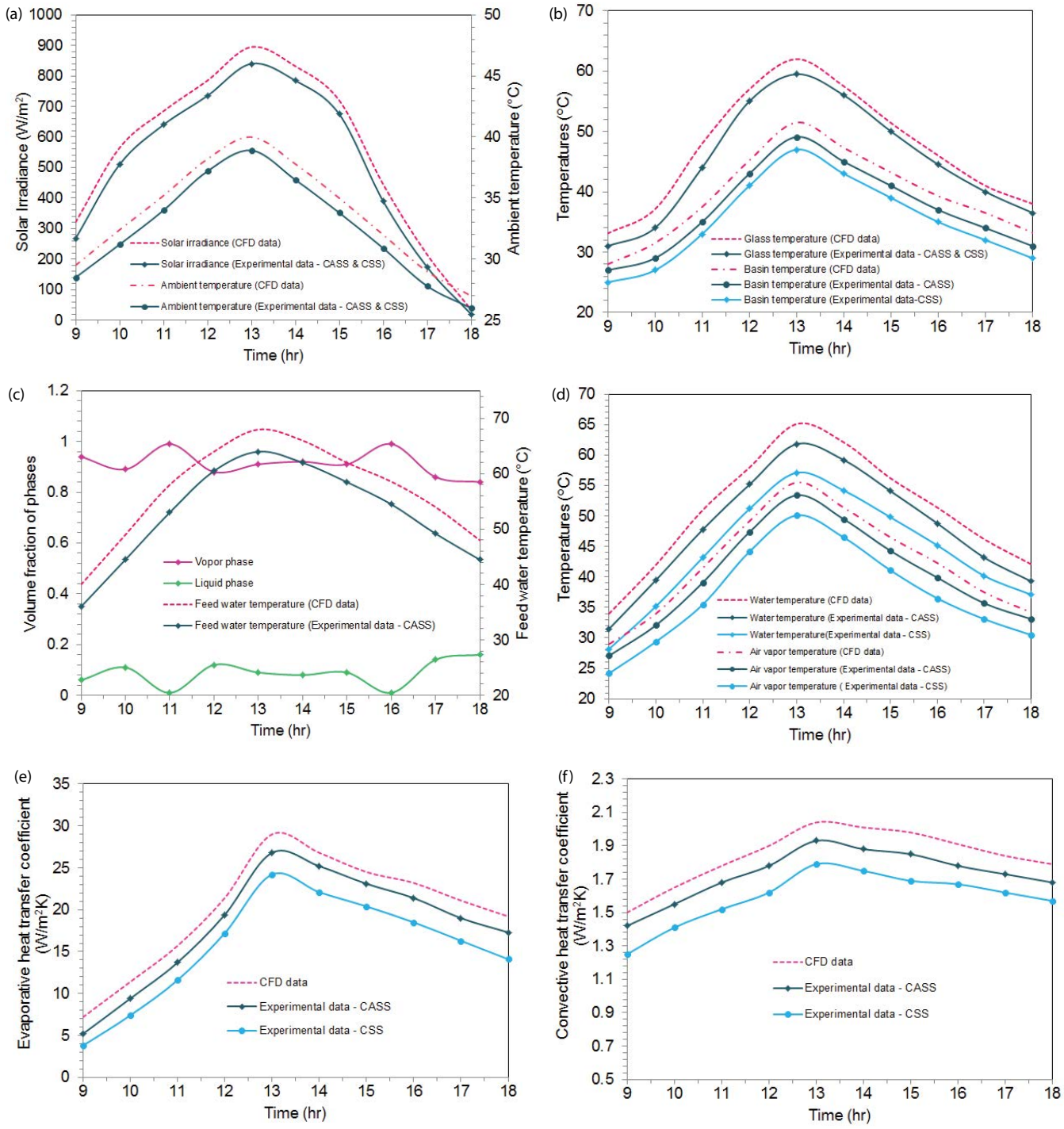

Fig. 5. (a) Variations of solar irradiation and ambient temperature. Effects of (b) glass and basin temperature, (c) feed water temperature and volume fraction of phase. Variations of (d) air-vapor mixture and water temperature, (e) evaporative heat transfer rate, and (f) convective heat transfer rate.

in the basin [8,42]. The deviation between simulation and experimental results were found to be about 5.5%.

The effect of feed water temperature and volume fraction of the phase is illustrated in Fig. 5c. It is observed that, the maximum preheated feed water temperature for both simulation and experimental are observed to be about 68.2°C and 64.1°C, respectively. In CSS, the feedwater temperature is relatively same to the ambient temperature conditions. Hence, it was not taken for the effect of feed water observation. The deviation observed from simulation results to experimental results was about 7.2% with the same flow patterns. For the volume fraction of the phase, it is observed

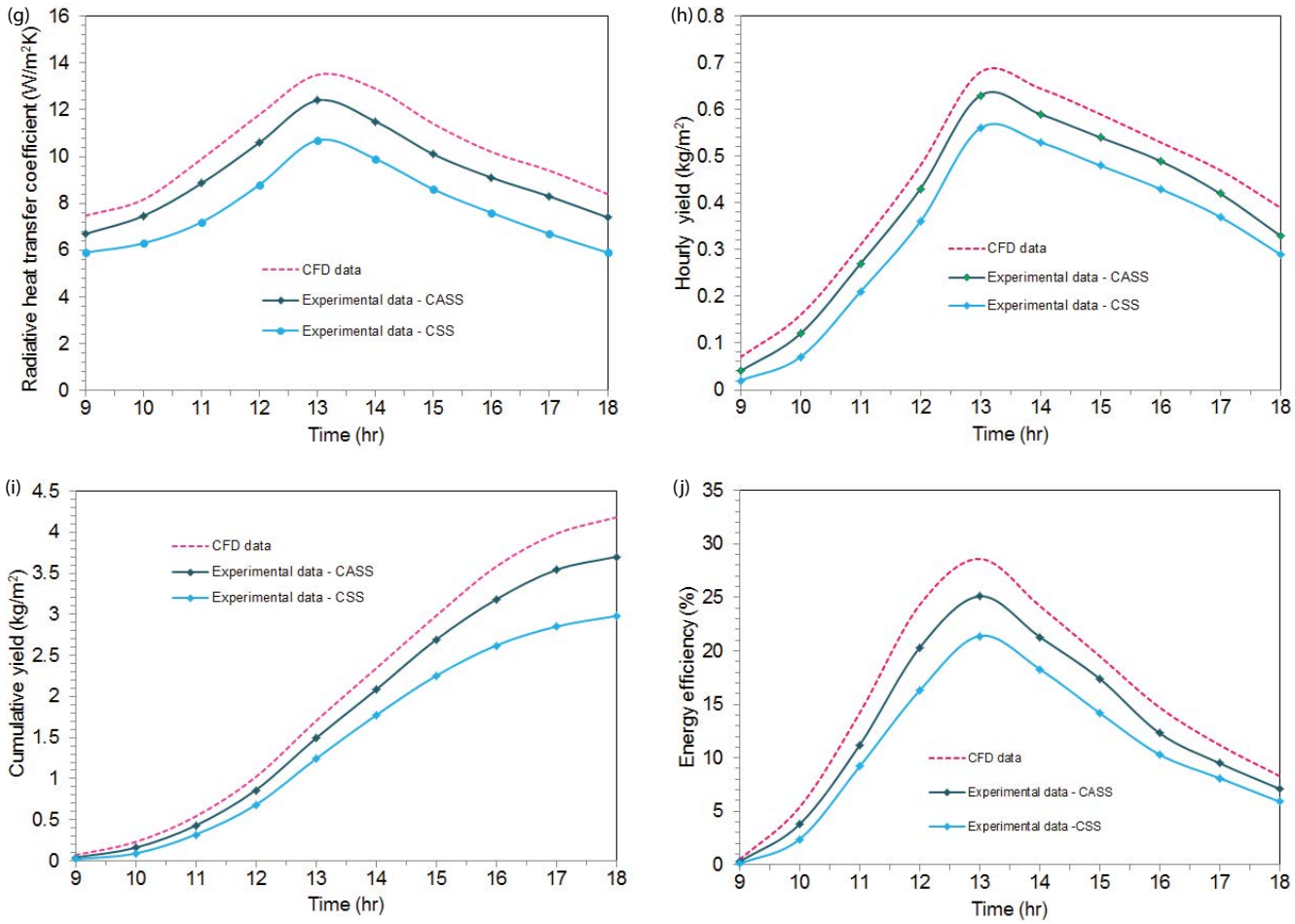

Fig. 5. Variations of (g) radiative heat transfer rate, (h) hourly productivity with time, (i) cumulative yield with time, and (j) energy efficiency with time.

that, the volume fraction of water was observed to be higher due to the absence of vapor during morning hours [40]. It increases significantly with the increase in temperature during peak sunshine hours. Finally, the water volume fraction is reduced to 0.02 during 18.00 h.

The variation of air vapor mixture and water temperature with time is depicted in Fig. 5d. It is observed that, the maximum air vapor temperature of simulation and experimental was about 55.5°C and 53.4°C respectively. In CSS, it is observed to be about 50.3°C. It is seen that, the air vapor mixture temperature of CASS was 5.8% higher than the air vapor mixture temperature observed from CSS. During late noon hours, the air vapor temperature reduces gradually when solar intensity decreases. This experimental observation also followed the similar patterns as that of simulation data. The deviation of simulation result from experimental result was about 8.4%. Also in Fig. 5d, the maximum saline water temperature for simulation and experimental was observed to be about 65.2°C and 62.3°C, respectively. In CSS, it was observed to be about 57.1°C. It is seen that, the water temperature of CASS was 8.3% higher than the water temperature observed from CSS. The rise in water temperature happens due to preheating of inlet saline water [8,16]. The deviation of water temperature from simulation to experimental was observed to be about 9.5%. But, the both results do follow the similar patterns.

The variations of evaporative heat transfer rate are depicted in Fig. 5e. It is observed that, the evaporation begins with low solar irradiations and by passing time preheated water in the CASS accelerates the evaporation. Since, the solar still space saturates with water vapor gradually, the evaporation rate enhances until about noon hours [40]. After that by decreasing solar irradiation, the distillate rate comes down slowly. It is observed that, the maximum evaporation rate for simulation and experimental were about 29.3 and 26.1 W/m²K, respectively. But in CSS, the maximum evaporative heat transfer rate was observed to be about 22.1 W/m²K which is 15.3% lower than the CASS. The variations of convective heat transfer rate are shown in Fig. 5f. It is observed that, the maximum convective heat transfer occurs during noon hours as solar irradiance increases. The highest value of convective heat transfer for simulation and experimental was observed to be about 2.04 and 1.93 W/m²K, respectively. But in CSS, the maximum convective heat transfer rate was observed to be about 1.76 W/m²K which is 7.9% lower than the CASS. Fig. 5g

illustrates the radiative heat transfer rate in solar still. It is observed that, the maximum radiative heat transfer rate for simulation and experimental were found to be about 13.5 and 12.4 W/m²K, respectively. For simulation, the radiative heat transfer rate was calculated using glass temperature and Stefan–Boltzman law [42]. The maximum radiative heat transfer rate of CSS was observed around 10.7 W/m²K which is 13.7% lower than the CASS. From Figs. 5e–g, it is seen that, the simulation and experimental results were followed the similar path. The deviation of evaporative, convective, and radiative heat transfer rate between simulation and experimental were 9.5%, 6.5%, and 10.6%, respectively.

Fig. 5h depicts the variation of the hourly productivity with time. It is observed that, the productivity starts slowly during morning hours and gradually increases in the noon hours as solar irradiation increase. The maximum yield of 0.68 and 0.61 kg/m² was observed in simulation and experimental results during 13:00 h. But in CSS, it was around 0.56 kg/m². The enhanced distillate of CASS was observed to be about 8.1% when compared to CSS. It happens due to the preheating technique in the CASS [8]. The deviation between simulation and experimental observation were about 14% and both the results do follow the similar patterns. Fig. 5i illustrates the variation of the cumulative yield with time. It is observed that, the simulation result showed the cumulative distillate of 4.31 kg/m² whereas the experimental was about 3.81 kg/m². The cumulative yield of CSS was observed to be about 2.92 kg/m² which is 23.3% lower than the productivity observed from CASS. It is also observed that, the experimental distillate of CASS was 3.41% higher than the earlier work reported in solar still using phase change materials [50]. The deviation between simulation and experimental observation were about 12.1% and both the results do follow the similar patterns. Fig. 5j depicts the variation of energy efficiency with time. It is noticed that, the maximum energy efficiency for simulation and experimental were observed to be about 28.6% and 25.1%, respectively. But in CSS, it was observed by 21.4%. The deviation between simulation and experimental observation were about 11.4% and both the results do follow the similar patterns. Finally, from Figs. 5a–j, it was observed that, the CFD prediction and experimental results were agreeable. The trends of variations in CFD prediction were similar to the experimental values.

6. Conclusions

In this work, a study has been attempted to develop a CFD model of a gravel coarse aggregate assisted single slope solar still and analyzed performance parameters with the experimental data under the same climatic conditions of Coimbatore city in India. The following major conclusions are drawn:

- In the simulation, a two-phase three-dimensional model has been developed using ANSYS FLUENT v19.2. Evaporation and condensation processes that are occurring in solar stills were also been simulated.
- The maximum water temperature for simulation and experimental were about 65.2°C and 62.3°C, respectively. The CASS water temperature was 8.3% higher than the water temperature observed from CSS.
- The maximum distillate of CFD prediction was about 4.31 kg/m² whereas the experimental was about 3.81 kg/m². The cumulative distillate of CSS was observed to be 23.3% lower than the CASS.
- The maximum energy efficiency of simulation and experimental were about 28.6% and 25.1%, respectively. The energy efficiency of CSS observed to be about 21.4%.
- Finally, CFD predicted results were compared with the experimental results. They were in good agreement with the maximum deviation of about 14%.
- By evaluating the experimental data in CFD simulations, the fresh water production rate doesn't change significantly, but it influenced on water temperature results.
- Predicted results of the CFD simulation show that, the computational fluid dynamics is a powerful tool for design, parameter analysis, and difficulties removal in solar still construction. In future work, the simulation can be done using different configuration in solar still.

Symbols

A	—	Solar still area, m²
D	—	Diffusion coefficient phases, m/s²
g_r	—	Gravity, m/s²
H	—	Specific enthalpy, J/kg
h	—	Heat transfer co-efficient, W/m²K
I	—	Solar irradiation, W/m²
L	—	Latent heat of evaporation, J/kg
M	—	Interface momentum transfer, kg/m²s²
m	—	Distillate output, kg
P	—	Pressure, N/m²
Q	—	Heat transfer between phases, W/m²
q	—	Enthalpy flux, W/m²
r	—	Volume fraction, dimensionless
S	—	Rate of mass transfer, kg/m³s
T	—	Temperature, K
U	—	Overall heat transfer co-efficient, W/m²K
V	—	Velocity vector, m/s
X	—	Mass fraction of liquid phase
Y	—	Mass fraction of gas phase

Greek

ε_{eff}	—	Effective emissivity
σ	—	Stefan-Boltzmann constant, 5.67×10^{-8} W/m²K⁴
μ	—	Viscosity, kg/ms
ρ	—	Density, kg/m³
η	—	Efficiency, %

Subscripts

c	—	Convection
ca	—	Coarse aggregate
eva	—	Evaporation
G	—	Gas
g	—	Glass
GL	—	Gas to Liquid
L	—	Liquid

LG — Liquid to Gas
o — Overall
r — Radiation
ss — Solar still
w — Water

References

[1] S.K. Suraparaju, S.K. Natarajan, Performance analysis of single slope solar desalination setup with natural fiber, Desal. Water Treat., 193 (2020) 64–71.
[2] M.H. Amirkalaei, A. Khoshgard, H. Ahmadi-Danesh Ashtiani, R. Fazaeli, Investigation of the parameters influencing the evaporation rate of downward sprayed sea water in solar water desalination, Desal. Water Treat., 191 (2020) 64–71.
[3] K. Hardik Jani, V. Kalpesh Modi, Experimental performance evaluation of single basin dual slope solar still with circular and square cross-sectional hollow fins, Sol. Energy, 179 (2019) 186–194.
[4] P. Dumka, A. Sharma, Y. Kushwah, A.S. Raghav, D.R. Mishra, Performance evaluation of single slope solar still augmented with sand filled cotton bags, J. Energy Storage, 25 (2019) 100888, doi: 10.1016/j.est.2019.100888.
[5] A.F. Mohamed, A.A. Hegazi, G.I. Sultan, E.M.S. El-Said, Enhancement of a solar still performance by inclusion the basalt stones as a porous sensible absorber: experimental study and thermo-economic analysis, Sol. Energy Mater. Sol. Cells, 200 (2019) 109958, doi: 10.1016/j.solmat.2019.109958
[6] V. Kalpesh Modi, H. Kuldeep Nayi, Efficacy of forced condensation and forced evaporation with thermal energy storage material on square pyramid solar still, Renewable Energy, 153 (2020) 1307–1319.
[7] E.M.S. El-Saida, S.M. Elshamy, A.E. Kabeel, Performance enhancement of a tubular solar still by utilizing wire mesh packing under harmonic motion, Desalination, 474 (2020) 114165, doi: 10.1016/j.desal.2019.114165.
[8] R. Dhivagar, S. Sundararaj, Thermodynamic and water analysis on augmentation of a solar still with copper tube heat exchange in coarse aggregate, J. Therm. Anal. Calorim., 136 (2019) 89–99.
[9] P. Zanganeh, A.S. Goharrizi, S. Ayatollahi, M. Feilizadeh, Productivity enhancement of solar stills by nano-coating of condensing surface, Desalination, 454 (2019) 1–9.
[10] A.E. Kabeel, M. Abdelgaied, A. Eisa, Effect of graphite mass concentrations in a mixture of graphite nanoparticles and paraffin wax as hybrid storage materials on performances of solar still, Renewable Energy, 132 (2019) 119–128.
[11] S.J.P. Gnanaraj, V. Velmurugan, An experimental study on the efficacy of modifications in enhancing the performance of single basin double slope solar still, Desalination, 467 (2019) 12–28.
[12] M. Sakthivel, S. Shanmugasundram, T. Alwarsamy, An experimental study on a regenerative solar still with energy storage medium – Jute cloth, Desalination, 264 (2010) 24–31.
[13] T.G. Sakthivel, T.V. Arjunan, Thermodynamic performance comparison of single slope solar stills with and without cotton cloth energy storage medium, J. Therm. Anal. Calorim., 137 (2019) 351–360.
[14] T.R.S. Kumar, S. Jegadheeswaran, P. Chandramohan, Performance investigation on fin tube solar still with paraffin wax as energy storage media, J. Therm. Anal. Calorim., 136 (2019) 101–112.
[15] A.A.M. Omara, A.A.A. Abuelnuor, H.A. Mohammed, M. Khiadani, Phase change materials (PCMs) for improving solar still productivity: a review, J. Therm. Anal. Calorim., 139 (2020) 1585–617.
[16] R. Dhivagar, S. Sundararaj, A review on methods of productivity improvement in solar desalination, Appl. Mech. Mater., 877 (2018) 414–429.
[17] S. Rashidi, N. Karimi, O. Mahian, A concise review on the role of nanoparticles upon the productivity of solar desalination systems, J. Therm. Anal. Calorim., 135 (2019) 1145–1159.
[18] A.E. Kabeel, A. Mohamed, M. Mahgoub, The performance of a modified solar still using hot air injection and PCM, Desalination, 379 (2016) 102–107.
[19] Y. Belyayev, M. Mohanraj, S. Jayaraj, A. Kaltayev, Thermal performance simulation of a heat pump asssited solar desalination system for Kazakhstan conditions, Heat Transfer Eng., 40 (2019) 1060–1072.
[20] K. Hidouri, R.B. Slama, S. Gabsi, Hybrid solar still by heat pump compression, Desalination, 250 (2010) 444–449.
[21] K. Hidouri, M. Mohanraj, Thermodynamic analysis of a heat pump assisted active solar still, Desal. Water Treat., 154 (2019) 101–110.
[22] H. Hassan, M.S. Yousef, M. Fathy, M. Salem Ahmed, Assessment of parabolic trough solar collector assisted solar still at various saline water mediums via energy, exergy, exergoeconomic, and enviroeconomic approaches, Renewable Energy, 155 (2020) 604–616.
[23] N. Rahbar, A. Gharaiian, S. Rashidi, Exergy and economic analysis for a double slope solar still equipped by thermoelectric heating modules - an experimental investigation, Desalination, 420 (2017) 106–113.
[24] S. Rashidi, N. Rahbar, M. Sadegh Valipour, J. Abolfazli Esfahani, Enhancement of solar still by reticular porous media: experimental investigation with exergy and economic analysis, Appl. Therm. Eng., 130 (2017) 1341–1348.
[25] C. Sasikumar, A.M. Manokar, M. Vimala, Experimental studies on passive inclined solar panel absorber solar still. J. Therm. Anal. Calorim., 139 (2020) 3649–3660.
[26] A.M. Manokar, M. Vimala, R. Sathyamurthy, Enhancement of potable water production from an inclined photovoltaic panel absorber solar still by integrating with flat-plate collector, Environ. Dev. Sustainability, 22 (2020) 4145–4167.
[27] S. Rashidi, J.A. Esfahani, N. Rahbar, Partitioning of solar still for performance recovery: experimental and numerical investigations with cost analysis, Sol. Energy, 153 (2017) 41–50.
[28] S. Rashidi, M. Bovand, J. Abolfazli Esfahani, Optimization of partitioning inside a single slope solar still for performance improvement, Desalination, 395 (2016) 79–91.
[29] A.A. El-Sebaii, A.A. Al-Ghamdi, F.S. Al-Hazmi, A.S. Faidah, Thermal performance of a single basin solar still with PCM as a storage medium, Appl. Energy, 86 (2009) 1187–1195.
[30] S. Rashidi, M. Bovand, J. Abolfazli Esfahani, Volume-of-fluid model for simulating vapor–liquid phase change in a solar still, J. Thermophys. Heat Transfer, 32 (2018) 1–7, doi: 10.2514/1.T5316.
[31] S. Rashidi, M. Bovand, N. Rahbar, J. Abolfazli Esfahani, Steps optimization and productivity enhancement in a nanofluid cascade solar still, Renewable Energy, 118 (2018) 536–545.
[32] A.M. Radhwan, Transient performance of stepped solar still with built-in latent heat thermal energy storage, Desalination, 171 (2004) 61–76.
[33] A.J. Chamkha, H.S. Takhar, V.M.Soundalgekar, Radiation effects on free convection flow past a semi-infinite vertical plate with mass transfer, Chem. Eng. J., 84 (2001) 335–342.
[34] H.M. Sadeghi, M. Babayan, A.J. Chamkha, Investigation of using multi-layer PCMs in the tubular heat exchanger with periodic heat transfer boundary condition, Int. J. Heat Mass Transfer, 147 (2020), doi: 10.1016/j.ijheatmasstransfer.2019.118970.
[35] A.J. Chamkha, Solar radiation assisted natural convection in uniform porous medium supported by a vertical flat plate, J. Heat Transfer, 119 (1997) 89–96.
[36] M.I. Ahmed, M. Hrairi, A.F. Ismail, On the characteristics of multistage evacuated solar distillation, Renewable Energy, 34 (2009) 1471–1478.
[37] N. Rahbar, J. Abolfazli Esfahani, E. Fotouhi-Bafghi, Estimation of convective heat transfer coefficient and water-productivity in a tubular solar still – CFD simulation and theoretical analysis, Sol. Energy, 113 (2015) 313–323.
[38] S. Rashidi, S. Akar, M. Bovand, R. Ellahi, Volume of fluid model to simulate the nanofluid flow and entropy generation in a single slope solar still, Renewable Energy, 115 (2018) 400–410.

[39] H.N. Panchal, N. Patel, ANSYS CFD and experimental comparison of various parameters of solar still, Int. J. Ambient Energy., 39 (2018) 551–557.
[40] V.R. Khare, A.P. Singh, H. Kumar, R. Khatri, Modelling and performance enhancement of single slope solar still using CFD, Energy Procedia, 109 (2017) 447–455.
[41] Y. Taamneh, Influence of Jordanian zeolite on the performance of a solar still: experiments and CFD simulation studies, Water Sci. Technol., 16 (2016) 1700–1709.
[42] R. Dhivagar, M. Mohanraj, K. Hidouri, Y. Belyayev, Energy, exergy, economic and enviro-economic (4E) analysis of gravel coarse aggregate sensible heat storage-assisted single-slope solar still, J. Therm. Anal. Calorim., (2020), doi: 10.1007/s10973–020–09766-w.
[43] N. Setoodeh, R. Rahimi, A. Ameri, Modeling and determination of heat transfer coefficient in a basin solar still using CFD, Desalination, 268 (2011) 103–110.
[44] Z.H. Yousef, K.A. Mousa, Modeling and performance analysis of a regenerative solar desalination unit, Appl. Therm. Eng., 24 (2004) 1061–1072.
[45] K.K. Murugavel, S. Sivakumar, J. Riaz Ahamed, Kn.K.S.K. Chockalingam, K. Srithar, Single basin double slope solar still with minimum basin depth and energy storing materials, Appl. Energy, 87 (2010) 514–523.
[46] V. Velmurugan, C.K. Deenadayalan, H. Vinod, K. Srithar, Desalination of effluent using fin type solar still, Energy, 33 (2008) 1719–1727.
[47] T. Mahmood, M.Y. Naz, S.A. Sulaiman, Y. Jamil, S. Shukrullah, M. Zahid, M. Inayat, CFD modeling and experimental validation of a solar still, MATEC Web. Conf., 131 (2017) 02010, doi: 10.1051/matecconf/201713102010.
[48] M.S. Yousuf, H. Hassan, An experimental work on the performance of the single slope solar still incorporated with latent heat storage system in hot climate conditions, J. Cleaner Prod., 209 (2019) 1396–1410.
[49] A.K. Raj, M. Srinivas, CFD modeling of macro-encapsulated latent heat stoarge system used for solar heating application, Int. J. Therm. Sci., 139 (2019) 88–104.
[50] H.N. Panchal, P.K. Shah, Modelling and verification of single slope solar still using ANSYS-CFX, Int. J. Energy Environ., 2 (2011) 985–998.